Bioelectrochemical platform with human monooxygenases: FMO1 and CYP3A4 tandem reactions with phorate

Bioelectrochemical platform with human monooxygenases: FMO1 and CYP3A4 tandem reactions with phorate

Hanna Cheropkina,[1] Gianluca Catucci,[1] Federico Cesano,[2,3] Arianna Marucco,[1] Gianfranco Gilardi,[1,3] Sheila J. Sadeghi[1,3]*

[1]Department of Life Sciences and Systems Biology, University of Torino, via Accademia Albertina, Torino 10123, Italy

[2]Department of Chemistry & INSTM-UdR Torino, Via Giuria 7, Torino 10125, Italy

[3]Centre for Nanostructured Interfaces and Surfaces, University of Torino, via Pietro Giuria 7, 10125 Torino, Italy

ABSTRACT

It is highly advantageous to devise an in vitro platform that can predict the complexity of an in vivo system. The first step of this process is the identification of a xenobiotic whose monooxygenation is carried out by two sequential enzymatic reactions. Pesticides are a good model for this type of tandem reactions since in specific cases they are initially metabolised by human flavin-containing monooxygenase 1 (hFMO1), followed by cytochrome P450 (CYP). To assess the feasibility of such an in vitro platform, hFMO1 is immobilised on glassy carbon electrodes modified with graphene oxide (GO) and cationic surfactant didecyldimethylammonium bromide (DDAB). Uv-vis, contact angle and AFM measurements support the effective decoration of the GO sheets by DDAB which appear as 3 nm thick structures. hFMO1 activity on the bioelectrode versus three pesticides; fenthion, methiocarb and phorate, lead to the expected sulfoxide products with K_M values of 29.5 ± 5.1, 38.4 ± 7.5, 29.6 ± 4.1 μM, respectively. Moreover, phorate is subsequently tested in a tandem system with hFMO1 and CYP3A4 resulting in both phorate sulfoxide as well as phoratoxon sulfoxide. The data demonstrate the feasibility of using bioelectrochemical platforms to mimic the complex metabolic reactions of xenobiotics within the human body.

Keywords: AFM, Flavoprotein, biocatalysis, graphene oxide, methiocarb, phorate, fenthion

1 Introduction

Pesticides are an integral part of agriculture for the prevention, control and elimination of pests. Yearly, more than 2.4 billion kilograms of broad-spectrum pesticides are used including mainly organophosphates, carbamates, organochlorines, neonicotinoids and pyrethroids [1]. But majority of pesticides are hazardous chemicals and increasing the field of their action has led to significant attention to their toxicity and adverse influence on the environment and human health. Chronic exposure to low levels of pesticides can cause mutations [2]. Among the many pesticides, organophosphates and carbamates have also been classified as carcinogens as well as neurotoxic causing neurodegenerative diseases such as Parkinson's [3-4] and Alzheimer's [5-6]. This has led to legislators imposing limits for the maximum residual amounts for individual pesticides of 0.1 µg/L [7].

Exposure to organophosphate and carbamate pesticides can occur in occupational settings but also in general public. In the case of the general public, the main routes of exposure include dermal, inhalation and diet [8]. Once they have entered the human body, pesticides are mainly metabolized by two major classes of Phase I oxidative enzymes: cytochromes P450 and flavin-containing monooxygenases (FMOs) [9]. Cytochrome P450 monooxygenases (CYPs) are a superfamily of haem-containing proteins whereas the FMO family is quite small with only 5 functional members which have a FAD cofactor [10-12]. Both families are NADPH dependent but FMOs are capable of accepting electrons directly from NADPH whereas CYPs require a NADPH reductase. Both enzyme families have been extensively studied in relation to the detoxification of pesticides. In the case of organophosphate pesticides, the P450 enzymes have been shown to be involved in oxidative transformations resulting in oxon, sulfoxide and sulfone [13] whereas the FMOs only produce sulfoxides [14]. Previous studies by Furnes and Schlenk have shown that amongst the 5 different FMO isoforms, the extrahepatic FMO1 primarily found in kidney and intestines, is the most efficient in catalysing the sulfoxidation of carbamate and organophosphate pesticides [15]. Other in vitro studies of pesticide metabolism mediated by hFMO1 have described the preference of this enzyme for oxidation of sulfur atoms with a high level of stereoselectivity and catalytic efficiency [15-17].

The main method for determination of the activity of these enzymes towards the pesticides has been the in vitro enzymatic assay where the reductant NADPH is added to initiate the reaction. An alternative method can be the use of electrodes where these enzymes are immobilised and which have successfully been applied to drug metabolism studies [18-20]. In

addition, in order to miniaturize the electrode and enhance the sensing characteristics, different nanostructured materials are widely used such as gold nanoparticles, graphene and its derivates. The main advantages of using nanostructured materials in enzyme electrodes is their efficient electrocatalyst properties, high surface area or surface-to-volume ratio and enhancement of electron transfer [21]. One such material is graphene oxide that has occupied a dominant place in the biosensing field due to its efficient electrochemical and catalytical properties [22-24].

In this work, human FMO1 (hFMO1) is initially immobilised on glassy carbon electrodes in the presence of graphene oxide (GO) for investigating the feasibility of following the oxidation of different pesticides by the enzyme. The GO is functionalised by the cationic surfactant dimethyldidodecylammonium bromide (DDAB) to avoid denaturation of this enzyme [25-26] and surface properties of functionalized GO sheets are investigated by contact angle and atomic force microscopy (AFM). Three well-known substrates of hFMO1, organophosphate pesticides phorate and fenthion as well as the carbamate insecticide, methiocarb, are chosen and voltammetric titrations are carried out for the determination of kinetic parameters. Subsequently and more interestingly, the possibility of mimicking the complexity of the in vivo metabolic reactions of phorate within the human body is investigated in an in vitro tandem bioelectrochemical set up with hFMO1 and CYP3A4 (cytochrome P450 3A4 the most important hepatic P450 in terms of xenobiotic metabolism). The data obtained confirm the possibility of using immobilised hFMO1 and CYP bioelectrodes for the in vitro prediction of the metabolic fate of pesticides.

2 Material and methods

2.1 Reagents

Riboflavin, FAD, IGEPAL, β-mercaptoethanol, glycerol, PMSF, lysozyme, NADPH, didodecyldimethylammonium bromide (DDAB), phorate, phorate S-oxide, phorate sulfone, fenthion, fenthion S-oxide, methiocarb, methiocarb S-oxide, acetonitrile, phosphoric acid, methanol, and salts were all purchased from Sigma-Aldrich. Phorate oxon sulfoxide was purchased from Toronto research chemicals, Canada. GO (4 mg/mL, water dispersion) was purchased from Graphenea (Donostia, Spain). PK-4 Polishing Kit and all supplements for

electrochemical measurements were from BASi (USA). All chemicals were of highest quality and used without any further purification. All media, solutions, and buffers were prepared with deionized Milli-Q water.

2.2 Purification of human FMO1

Human FMO1 was expressed in Escherichia coli JM109 cells in 2 L conical flasks containing 500 mL Terrific Broth in the presence of ampicillin (100 μg/mL) and riboflavin (50 mg/L) as described previously [27]. After expression, the protein was purified from the membrane fractions via DEAE anion-exchange and Ni- chelating Sepharose fast-flow affinity column, following the procedure described previously [28]. The concentration and yield of obtained FMO1 protein were estimated by UV/Vis spectroscopy considering a 1:1 molar content of FAD. Protein purity was verified by separation and visualization in a 12% SDS polyacrylamide gel stained with Coomassie Blue. The activity of the purified FMO1 was determined by the methimazole assay described by Catucci and co-workers [29].

2.3 In vitro metabolic assay

To estimate kinetic parameters for S-oxygenation of pesticides mediated by hFMO1, reactions were set up in a final volume of 200 μL in 50 mM potassium phosphate buffer pH 8.0 containing 0.5 μM enzyme, 0.5 mM NADPH and different concentrations of pesticide from 0 to 200 μM. The reaction was initiated by adding NADPH and incubated at 37 °C for 30 min. The reactions were terminated by adding 100 μL of ice-cold acetonitrile. After protein precipitation the mixture was centrifuged at 12000 × g for 5 min and the supernatant was analysed by HPLC to identify the metabolite(s) formed.

2.4 High-Performance Liquid Chromatography

The separation and quantitation of the reaction mixtures were performed by using a calibration curve of analytical standards of substrates (phorate, methiocarb, fenthion) and products (phorate S-oxide, methiocarb S-oxide, fenthion S-oxide). The analysis was performed with an Agilent 1200 quaternary pump HPLC System equipped with a diode array UV detector (Agilent Technologies, USA) with a Kinetex 5 μm EVO C18 100Å column 250 × 4.6 mm. Pesticides and their metabolites were separated by gradient elution consisting of A – acetonitrile and B – 10 mM phosphoric acid

as follows: A – 5%, B – 95% (0-2 min); A – 95%, B – 5 % (18 min); 20 min: A – 95 %, B – 5 %; 23 min: A – 5 %, B – 95 %; 30 min: A – 5 %, B – 95 %. All metabolites were detected at a wavelength of 210 nm at a flow rate of 1 mL/min. The retention time of pesticides and their metabolites were: phorate 17.2 min, phorate S-oxide 12.7 min; methiocarb 13.7 and 14.2 min (commercially obtained compound had two peaks), methiocarb S-oxide 8.3 min; fenthion 16.5 min, fenthion S-oxide 12.2 min.

2.5 Preparation of DDAB functionalized graphene oxide (GO-DDAB)

For the preparation of DDAB-GO, 100 mM DDAB water solution with 1 mg/mL of GO dispersion was sonicated for 30 min to obtain a homogeneous dispersion. After this, the mixture was heated at 80 ºC for 1 hour to achieve the ionic functionalization of GO by cationic surfactant DDAB [30]. After cooling down the obtained mixture was used for electrode modification and FMO1 immobilization without any additional washing or preparation steps.

2.6 Contact angle measurement

Contact angle data were obtained using Kruss Easy Drop DSA100 (Hamburg, Germany) and analyzed by the Drop Shape Analysis software. Silicon wafers were cleaned using isopropanol and placed in a sonicator bath for 10 minutes and then rinsed with milli Q water. Initially, 20 µl of 1 mg/ml GO solution was placed on the wafer and after evaporation the static contact angle was measured. In the second experiment, 20 µl of a solution DDAB-GO prepared as described above, was placed on the silicon wafer. Also in this case, after the sample had dried the static contact angle was measured with the following parameters: sessile water drop with constant drop volume, volume dispensed 10 µl, needle diameter 1 mm (thin), setting of Young Laplace equation for the data analysis. The data obtained are the mean of three independent experiment in which the value of the angle obtained is the mean of 10 acquisitions.

2.7 Atomic force microscopy

AFM measurements were carried out in the intermittent contact mode using a 225 µm long super-sharp Si cantilever (Nanosensors, SSS-NCL), having a tip radius of approximately 5 nm, which was mounted on a Nanosurf Easyscan2 AFM instrument equipped with a high-resolution

scan head (10 x 10 μm). The instrument, shielded in an insulated enclosure, was placed on an antivibration platform. Before analysis, 2 μl of GO sheets dispersed in water (final concentration 1 mg/ml), were dropped on a freshly cleaved mica support. Scan speed was 0.25 Hz with an image resolution of 256 × 256 pixels. Root-mean-square roughness (Rrms) was determined by measuring only the atop surface of sheets. Height distribution diagrams and Abbott-Firestone curves were determined on a selected regions of the AFM images.

2.8 Electrode preparation

All electrodes, 3.0 mm working glassy carbon electrode (BASi, USA), were mechanically polished with PK-4 polishing kit before each experiment. The working glassy carbon electrodes were subsequently modified with 5 μL of 100 mM DDAB water solution [31] or 5 μL GO-DDAB. This was followed by addition of 5 μL of purified hFMO1 (50 μM) onto the modified electrode surface and overnight incubation at 4 °C.

2.9 Cyclic Voltammetry and pesticide titration

Electrochemical measurements of immobilized hFMO1 in DDAB and/or GO-DDAB modified electrodes were performed in a three-electrode standard electrochemical cell with C-2 low-volume sample chamber, 0.5 mm platinum coil auxiliary electrode and Ag/AgCl (3 M NaCl) reference electrode. Working electrolyte consisted of 50 mM potassium phosphate buffer pH 8.0 and 0.1 M KCl. Measurements were carried out using an Autolab PGSTAT12 controlled by Nova 2.1 software (Metrohm / Ecochemie, The Netherlands) at room temperature.

Cyclic voltammograms of hFMO1 were performed under anaerobic conditions in a glovebox (Belle Technologies, UK) with nitrogen atmosphere. Scans were recorded from 0 to -750 mV with different scan rates from 20 to 120 mV/s.

For the titration experiments with different pesticides (increasing concentrations from 0 to 280 μM) the electrochemical response of the immobilized hFMO1 was measured after each addition of the pesticide. The electrochemical cell had a total volume of 500 μl with 50 mM potassium phosphate buffer pH 8.0 and 0.1 M KCl. After each addition the solution within the electrochemical cell was vigorously stirred for a couple of minutes to minimize mass

transport effects and the cyclic voltammogram recorded.

2.10 Tandem chronoamperometry with immobilised hFMO1 and CYP3A4

For the tandem chronoamperometry experiments, CYP3A4 was heterologously expressed in E. coli for 48 h and purified using two chromatography steps as described previously [18, 32]. The purified enzyme was subsequently immobilised on glassy carbon (GC) electrodes modified with poly (diallyldimethylammonium) (PDDA) polymer in a 1:1 mixture of PDDA:enzyme (25 μM) also described by our group [33].

The tandem chronoamperometry reactions were carried out in the presence of oxygen with continuous stirring at 200 rpm to prevent the mass transport limitations and saturation of the reaction products near the surface of the working electrode, at the optimal reaction temperature of 37 °C. Cyclic voltammetry was carried out before and after each chronoamperometric experiment to estimate the stability of the bioelectrodes. The chronoamperometry measurements were carried out in 500 μl of 50 mM potassium phosphate buffer pH 8.0 and 0.1 M KCl at a set potential of -650 mV (vs. $Ag/AgCl_2$). Initially, the chronoamperometry was carried out with the immobilised FMO1 on GC-DDAB-GO in the presence of phorate (final concentration of 500 μM) in the 3-electrode electrochemical cell described above. After 30 min of the reaction at 37 ºC, the electrode with immobilised hFMO1 was replaced by a new GC electrode, this time with CYP3A4 immobilised. Before starting the second chronoamperometry experiment, a 100 μl sample of the electrochemical cell solution was taken for HPLC analysis. Again, the chronoamperometry experiment was carried out at the same potential bias for another 30 min at 37 ºC after which time a second sample was taken for HPLC separation and analysis.

For the HPLC analyses, a 10 mM stock solution of phorate and its metabolites was prepared in the methanol and diluted to 100 μM in 0.1 M phosphate buffer pH 7.4. Prior to HPLC analysis the samples were further diluted 2:1 with the acetonitrile. The HPLC analysis was performed with an Agilent 1200 quaternary pump HPLC System equipped with a diode array UV detector (Agilent Technologies, USA) with a Kinetex 5 μm EVO C18 100Å LC column 250 × 4.6 mm. Phorate and its metabolites were separated by gradient elution with the required post-analysis washing step. The mobile phase consisted of A – acetonitrile and B – 10 mM Phosphoric acid. Gradient profile was: 0-2 min: A – 5 %, B – 95 %; 20 min: A – 95 %, B – 5 %; 23 min: A – 5 %, B – 95 %; 30 min: A – 5 %, B – 95 %. All metabolites were

detected at a wavelength of 210 nm at a flow rate of 1 mL/min. The retention times were: phorate – 17.2 min, phorate sulfoxide – 12.7 min, phorate sulfone – 14.3 min, phorate oxon sulfoxide – 9 min.

3 Result and discussion

3.1 In vitro measurement of kinetic parameters for selected pesticides and hFMO1

Human FMO1 was purified through two sequential chromatography steps as outlined in the methods section. It was then characterized by spectroscopy where the characteristic FAD cofactor absorbance maxima at 375 nm and 450 nm were observed. The spectrum was also used for the calculation of the yield of the expressed protein as well as concentration of the protein for subsequent *in vitro* experiments.

Subsequently, the *in vitro* metabolism of carbamate and organophosphate pesticides mediated by hFMO1 was investigated using three compounds namely phorate, fenthion and methiocarb. The chemical structures of these pesticides and their corresponding oxygenated products are shown in Figure 1. Phorate is an organophosphate insecticide widely used in crops such as corn, potato, cotton, wheat and peanuts. Fenthion, another organophosphate insecticide has low solubility in water but is highly soluble in organic solvents. It is used in post-harvest treatment of fruits and vegetables. It is moderately toxic to humans but highly toxic to birds. Both phorate and fenthion act via cholinesterase inhibition [34-35]. The third pesticide, methiocarb, is a carbamate insecticide. Due to its toxicity (also an acetylcholinesterase inhibitor), methiocarb approval as a plant protection product has been withdrawn by the EU effective 2020 [36].

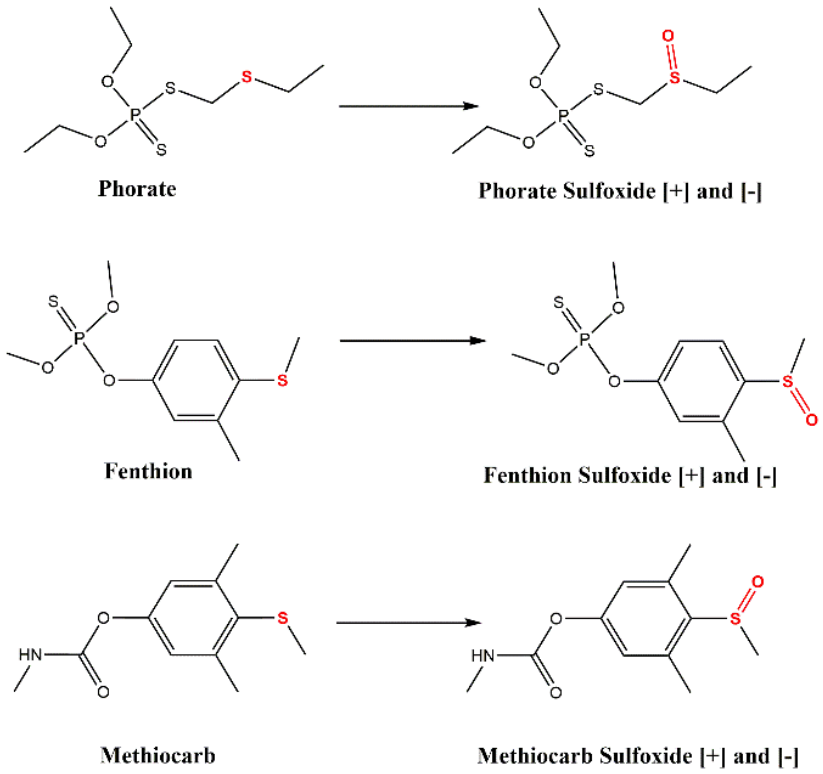

Figure 1: The chemical structures of the three investigated pesticides and their conversion to sulfoxides mediated by hFMO1.

The kinetic parameters K_M and V_{max}, for each of the three pesticides were measured with purified hFMO1 as described in the methods section. For each pesticide, different concentrations were used with of hFMO1 and with the addition of NADPH. Reactions were carried out at 37 ºC for 30 min after which time the product(s) was separated and analysed by HPLC. Typical HPLC chromatograms obtained are shown in Figure 2. Phorate and its S-oxide have the retention times of 17.2 and 12.7 min , fenthion and its S-oxide 16.5 and 12.2 min and methiocarb and its S-oxide 13.7,14.2 and 8.3 min, respectively. As can be seen in figure 2, methiocarb and to a lesser extent, phorate and fenthion, were all actually present in two forms in the commercially obtained samples. However, in all cases hFMO1 is highly stereoselective only producing one product consistent with previous reports [17, 37-38]. In the specific case of phorate, Hodgson and colleagues have previously shown that hFMO produces predominantly the (+) stereoisomer [37]. In this study, we did not embark on separating the isomers and used the commercially available standards to identify the

sulfoxide.

The K_M values calculated for the *in vitro* conversion of phorate, fenthion and methiocarb to their corresponding oxygenated products by purified hFMO1 were 93 ± 14 µM, 87 ± 36 µM and 98 ± 16 µM, respectively. Different K_M values ranging from 30 to 340 µM have been reported previously [15-17] using human liver microsomes and these differences might be attributed to the source of the enzymes as well as the solubility of the pesticides used.

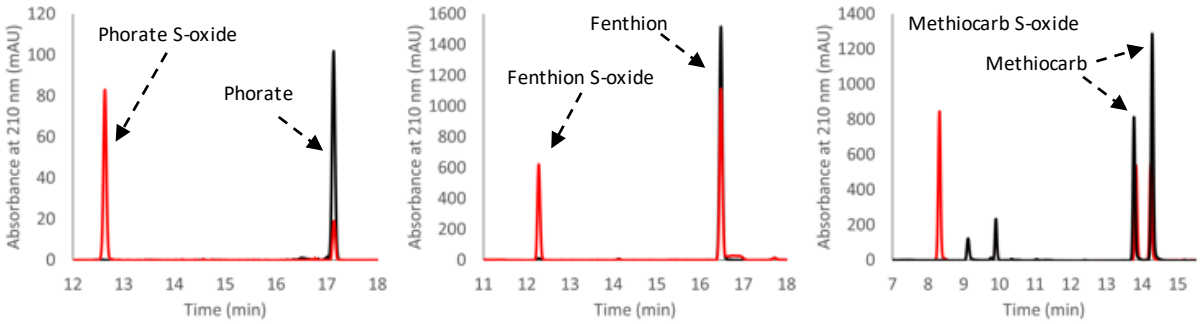

A B C

Figure 2: HPLC chromatograms of the separation of the *in vitro* sulfoxidation products obtained from the incubations of the three pesticides with hFMO1 (red line) and the respective control experiments in the absence (black line) of hFMO1. Reaction were carried out in a final volume of 200 µL in 50 mM potassium phosphate buffer pH 8.0 containing 0.5 µM enzyme, 0.5 mM NADPH and 200 µM of phorate **(A)**, fenthion **(B)** and methiocarb **(C)**.

3.2 Immobilisation of hFMO1 on glassy carbon electrodes

The *in vitro* enzymatic assay of hFMO1 with the 3 pesticides was followed by the investigation of the same reactions but with the enzyme this time entrapped/immobilised on glassy carbon electrodes. To this end, the cationic surfactant DDAB, which we have successfully used for another human FMO, hFMO3 [25-26, 39-40], was used with or without the addition of GO. The presence of GO and its interaction with the DDAB was investigated using different methodologies including UV/Vis spectroscopy, contact angle and AFM.

Initially, the functionalization of DDAB by GO was followed by UV/Vis spectroscopy and the data obtained are shown in Figure 3A. As can be seen in the figure, the main GO absorption peaks at 233 nm corresponding to π-π* transition of the C-C aromatic bonds, and 305 nm corresponding to n-π* transition of C=O bonds are totally lost in the GO-DDAB

spectrum [41]. Since the GO fingerprints are completely absent in DDAB-GO spectrum this implies not only that GO is attached to the DDAB but also its surface is entirely covered by DDAB.

The hydrophilicity of the GO-DDAB was analysed by contact angle measurements and compared to the GO water suspension. This methodology allows for the quantitative measurement based on intermolecular interactions between the surface already functionalized by GO or GO-DDAB and a small drop of water in contact with it. It is mainly used for assessing the wettability of a surface but here it was used to determine any changes regarding the hydrophobicity of the GO-DDAB. The contact angle results are shown in Figure 3B-C. As can be seen in the figure, the GO water suspension as expected is hydrophilic in character and thus results in very low water contact angle i.e. 8.0 º ± 0.71. On the other hand, the addition of the DDAB causes an increase in the hydrophobicity of the resulting GO-DDAB layer and therefore water contact angle of 46º ± 0.19 is observed. This value is in line with data published previously [30]. The observed increase in hydrophobicity is advantageous for the immobilisation of hFMO1 since this protein, similar to hFMO3, has a predicted hydrophobic group of amino acids at its C-terminal which anchor it to the ER membrane [42]. The latter being the reason behind purifying this protein from membrane fractions and not the *E. coli* cytosol.

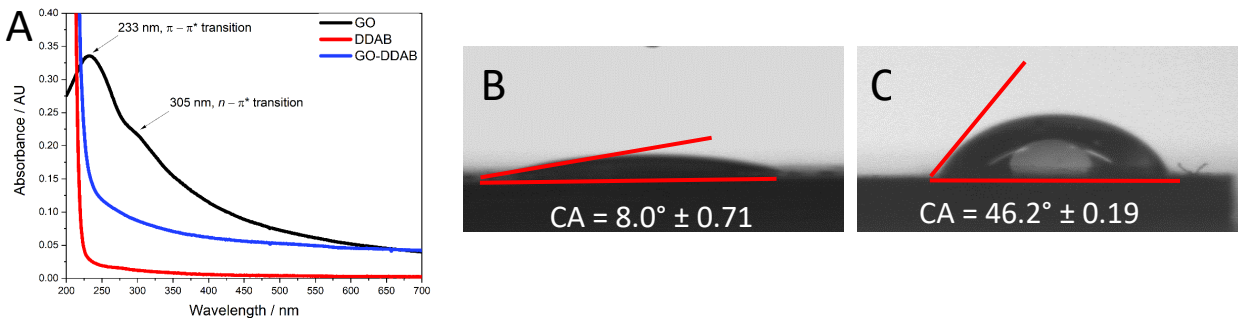

Figure 3. UV/Vis absorbance spectra of modified GO by cationic surfactant DDAB (A). Contact angles of water droplets on the surface of GO (B) and GO-DDAB deposited films (C). The red bars demonstrate the changes in the angles measured.

3.2.1 Atomic Force Microscopy (AFM)

The surface properties of GO and of DDAB-grafted GO sheets were investigated by means of AFM. Morphological signals, height profiles along selected lines, and height distributions are shown in Figure 4, respectively. In Figure 4a, a few GO sheets are AFM imaged. From this figure it is clear that the majority of the sheets had lateral sizes in the 0.5-1 μm range, but smaller sheets were also present. The root-mean-square average of the profile height deviations from the mean line value (R_{rms}) [43] of the top surface of GO sheets was calculated to be 249 pm. The height profiles of about 1 and 2 ± 0.1 nm measured along two selected lines (Figure 4b) are typically observed for single-layered (1L) and bilayered (2L) GO sheets, respectively. The height distributions of a region selected in Figure 4a (red histogram in Figure 4c) revealed three peaks with Gaussian profiles with maxima spaced of 0.9 ± 0.05 nm. Such peaks can be safely assigned to the atop height of the mica support, 1L- and 2L-GO sheet thicknesses, respectively. A surface statistical approach was then performed by processing the cumulative distribution function of the surface heights (known as Abbott-Firestone curve or bearing curve) [44]. As shown in Figure 4c (black curve), the cumulative curve of heights showed a distinctive profile with three roughly vertical steps in the 0.4-1.0 ± 0.1 nm interval for ~66 % of the bearing area, a second increment in the 1.3-2.0 ± 0.1 nm corresponding to the ca. 95% of the surface, and a third and smaller increment of 2.3-2.7 ± 0.1 nm corresponding to ca. 99.8 % of the bearing area. In summary, these bearing area values are representative of the predominance of 1L-GO in comparison with 2L-GO sheets, and a quasi-negligible contribution of multi-layered GO sheets can be highlighted (1L-GO > 2L-GO >> multi-layered- GO sheets).

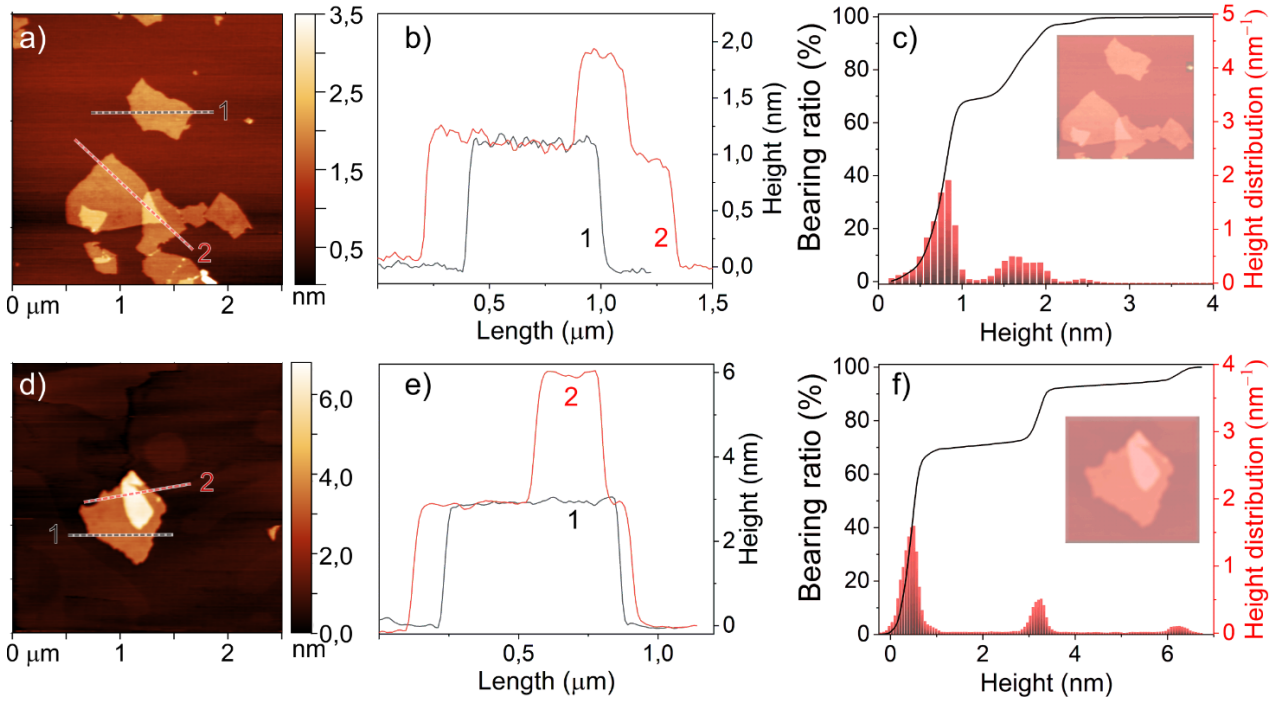

Figure 4 a) AFM image of GO sheets deposited on the mica support, b) related height profiles along two selected lines, c) height distribution (red histogram) and Abbott-Firestone curve (black line) of a selected region in a); d) AFM image of DDAB- grafted GO sheets deposited on the mica support, e) related height profiles along two selected lines, f) height distribution (red histogram) and Abbott-Firestone curve (black line) of a selected region in d).

In Figure 4d, two DDAB-functionalized GO sheets are AFM imaged. In this figure the sheets with lateral sizes in the 0.3-0.5 and 1 µm range are shown. Height profiles of about 2.9 and of 6.0 ±0.1 nm were measured along two selected lines shown in Figure 4d. Such heights could correspond to multi-layered GO and/or DDAB fully covering the GO sheets. However, from the comparison between R_{rms} value of GO sheets (GO R_{rms} = 249 pm) with the same value of DDAB-GO sheets (DDAB-GO R_{rms} = 1.26 nm) an increase of the R_{rms} of one order of magnitude is observed. Such increase in R_{rms} could be associated with the DDAB layer forming a rougher surface on the sheets, as also previously reported for Au surfaces modified with benzenethiol derivatives [45]. The height distributions of a region selected in Figure 4d (red histogram in Figure 4e) revealed three peaks with Gaussian profiles with maxima spaced of 2.75 ± 0.1 nm. Such peaks can be safely assigned to the atop heights of the mica support and of DDAB-functionalized-GO sheets of different stacking order, respectively. The Abbott-Firestone curve or is shown in Figure 4f (black curve), the cumulative curve of heights

showed a distinctive profile with three vertical steps in the 0.1-0.8 ± 0.1 nm interval with ~67 % of the bearing area, a second increment in the 2.9-3.4 ± 0.1 nm corresponding to the ca. 91.5% of the surface, and a third smaller increment of 6.0-6.6 ± 0.1 nm corresponding to ca. 99.5 % of the bearing area. In summary, these bearing area ranges are representative of a rougher surface after the functionalization with DDAB.

In conclusion, based on UV-Vis spectra, contact angle and AFM measurements, a structure model of DDAB-GO system can be schematized (Figure 5). In this figure, GO with oxygen-containing groups (-COOH, -OH, >C=O) located at the edges and epoxy groups on the basal planes of the GO structural unit is shown, thus behaving as an amphiphilic system with hydrophobic basal planes and hydrophilic edges [46]. The GO amphiphilic nature takes place at pH =< 7 with -COOH protonated species or pH > 8-9 with the carboxylate anions (–COO-), respectively [47-48]. From this structure model it is clear that, due to the interaction of DDAB with GO sheets on the basal planes with the Br ions far away and the long aliphatic chains facing GO sheets, an effective decoration of the GO sheet is observed. Such DDAB-decorated GO system appears about 3 nm thick in line with the AFM data.

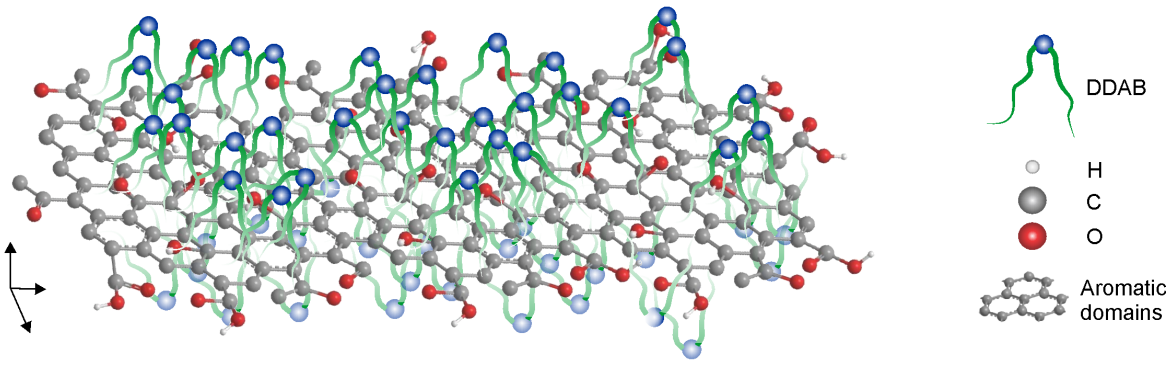

Figure 5: The structure model of DDAB-GO

3.3 Electrochemical behaviour of immobilized hFMO1

Characterization of redox properties of immobilized hFMO1 on modified GC electrodes was performed by cyclic voltammetry under anaerobic conditions to prevent spontaneous regeneration of enzyme-bound FAD cofactor to its oxidized form. Measurements were performed on both DDAB

and GO-DDAB modified electrodes (Figure 6) and the results obtained are summarized in Table 1. As expected in the control experiments, electrodes without immobilized enzyme, no redox peaks were observed (data not presented).

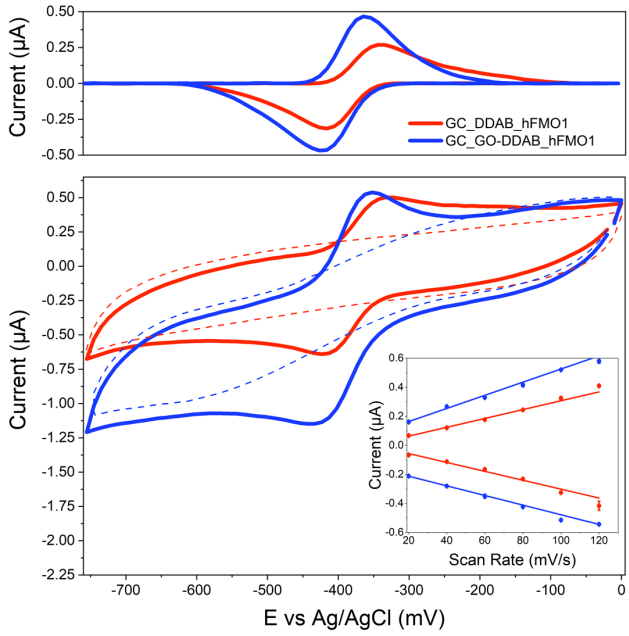

Figure 6: Cyclic voltammograms of hFMO1 immobilized on GC electrodes modified by DDAB in the presence (blue line) and absence (red line) of GO at scan rate of 100 mV/sec. The corresponding control cyclic voltammograms of GC electrodes modified with DDAB (dashed red) and DDAB-GO (dashed blue) are also shown. Bottom panel are original cyclic voltammogram with the linear dependence of current versus scan rate shown in the insert. Cyclic voltammograms in the top panel are baseline corrected.

Electrochemical reduction and oxidation process of immobilized hFMO1 demonstrated a reversible behaviour in both presence and absence of GO. The linear dependence of increasing current as a function of scan rate (up to 120 mV/s) shown in Figure 6 inset, is indicative of a thin-film confined electroactive species that are not under diffusion control as stated by Laviron's theory [49]. Midpoint potentials of the immobilised hFMO1 were -379 ± 3 and -395 ± 2 mV in the absence and presence of GO, respectively. Similar midpoint potentials were observed with hFMO3 immobilised on GC electrodes modified with DDAB [25]. Since the presence of GO resulted in higher observed currents, the number of electroactive species in the absence and presence of the GO were determined using the Laviron equation [49] by integration of the reduction peaks of the cyclic voltammograms. The surface coverage on GC-DDAB and GC-DDAB-GO were calculated to be 7.0 x 10^{12} and 1.3 x 10^{13} molecules/cm^2, respectively.

Table 1 Redox properties of immobilized hFMO1 on modified electrodes [#]

Electrode	E_{Ox} (mV)	E_{Red} (mV)	ΔE (mV)	$E_{1/2}$ (mV)
GC-DDAB-hFMO1	-346 ± 6	-412 ±2	66 ± 7	-379 ±3
GC-GO-DDAB-hFMO1	-364 ± 2	-425 ± 1	61 ± 2	-395 ± 2

Data obtained from cyclic voltammograms of hFMO1 under anaerobic conditions in a glovebox at room temperature. Scans were recorded from 0 to -750 mV with different scan rates from 20 to 120 mV/s in 50 mM phosphate buffer pH 8.0 and 0.1 M KCl.

3.4 Voltammetric titration of pesticides

The efficiency of modified GC/GO-DDAB/hFMO1 in the conversion of the three pesticides was investigated and the kinetic parameters determined. The electrode response was recorded in the presence of increasing pesticide concentration. Control measurements were carried out in the absence of immobilized protein (data not shown). The proportional increase of cathodic peak current simultaneously with pesticides concentration corresponds to enzyme catalytic activity of substrate oxygenation by using molecular oxygen dissolved in buffer, reducing equivalent and electrons from the electrode.

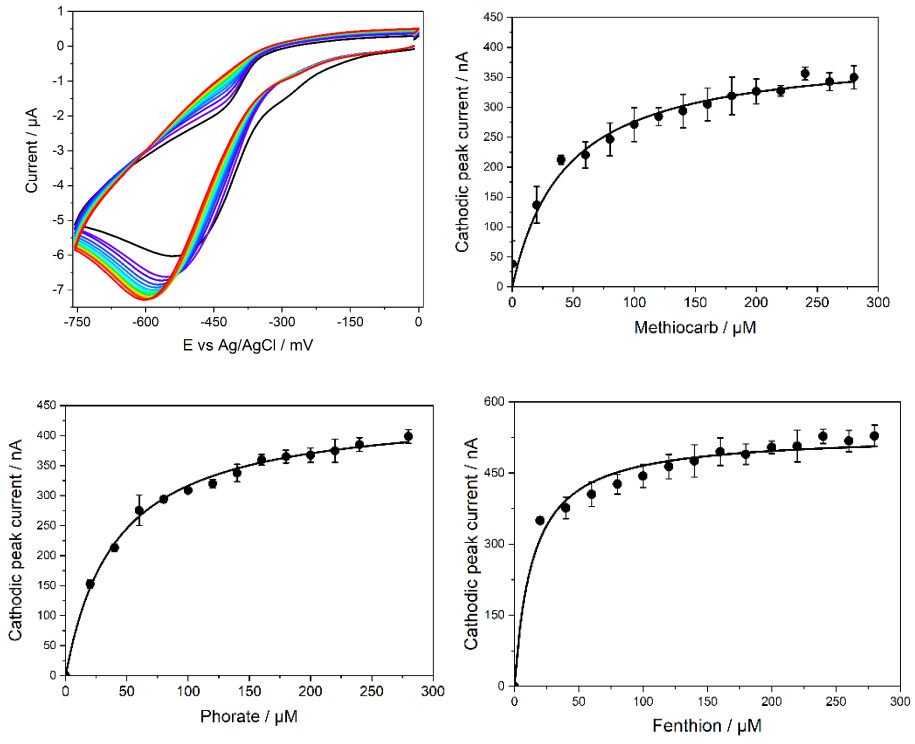

Figure 7: Typical cyclic voltammograms of hFMO1 immobilised on glassy carbon electrode modified with GO-DDAB titration with increasing pesticide concentrations from 0 μM (black line) to 280 μM (red line) in the presence of oxygen (**A**). Normalized catalytic current values as a function of the concentration of the pesticide added: Methiocarb **(B)**, Phorate **(C)** and Fenthion **(D)** fitted to the Michaelis-Menten equation. Estimated standard errors of three different electrode measurements are represented as error bars.

Human FMO1 immobilised on electrode and the resulting response to titration with increasing concentrations of each of the three pesticides, methiocarb, fenthion and phorate was followed by cyclic voltammetry. The obtained increases in the cathodic peak current upon addition of the pesticides was subsequently plotted against the known concentration of each pesticide in order to calculate the relevant kinetic parameters of hFMO1 modified electrodes by fitting the data to the Michaelis-Menten equation (Figure 7). The calculated apparent K_M values for fenthion, methiocarb and phorate were 29.5 ± 5.1 μM, 38.4 ± 7.5 μM, 29.6 ± 4.1 μM, respectively.

Kinetic values obtained for the conversion of the pesticides by the immobilized hFMO1 were compared to the *in vitro* data from the present work as well as previously published data [15-17, 37-38]. In general, the K_M values are within the same order of magnitude although for fenthion the values show larger variations. More studies need to be carried out to clarify the reasons behind these differences but one parameter could be the source and preparation of the enzyme as well as the assay conditions.

3.5 Bioelectrochemical tandem reactions of hFMO1 and Cytochrome P450 3A4 with phorate

Previously, Levi and Hodgson [37] have shown the conversion of phorate to different oxidation products with FMO and cytochrome P450s, a summary of which is shown in Figure 8. According to the latter researchers [37] hFMO1 is able to convert phorate (1) exclusively to phorate sulfoxide (2), whereas cytochrome P450 can potentially transform it to other additional oxidation products including phoratoxon sulfone (3) (via the intermediate phorate sulfone) and phoratoxon sulfoxide (4) (Fig. 8).

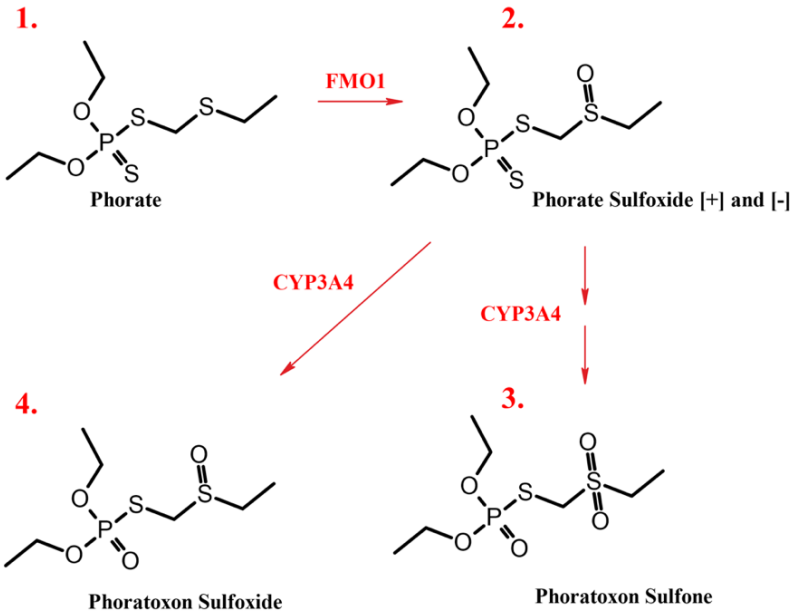

Figure 8. Scheme of FMO and CYP reactions involved in phorate oxidation [37].

Therefore, we investigated the possibility of performing an electrochemically-driven tandem reaction exploiting two immobilized enzymes on different electrodes working on a single reaction mixture. Initially, phorate was added to hFMO1 immobilized on DDAB-GO glassy carbon electrode and chronoamperometry was carried out for 30 min by applying a potential bias of -650 mV in the presence of oxygen. An aliquot of the reaction was then withdrawn from the mixture and HPLC separation revealed the expected phorate sulfoxide product (2) as shown in Figure 9. The same reaction mixture was then further subjected to electrocatalysis using a cytochrome P450, human hepatic CYP3A4 immobilized on glassy carbon electrode modified with PDDA (refer to methods section for details). CYP3A4 has been previously shown to carry out the different oxidation steps of phorate metabolism [17] although the main cytochrome P450 indicated in phorate transformation is 2C9 [17]. The reaction with immobilised CYP3A4 was carried out for a further 30 min as before. The HPLC separation in this case shows that the addition of this second step leads to the formation of two extra products: phoratoxon sulfone (3) and phoratoxon sulfoxide (4). Phoratoxon sulfone was not available as a pure standard therefore we inferred its presence from a previously published HPLC separation containing the same analytes [37]. As expected the amount of phorate sulfoxide (2) in the tandem reaction is increased due to the fact that CYP3A4 can also perform the same S-oxygenation reaction carried out by FMO1 but at a lower rate [17] (Figure 9). Nevertheless, CYP3A4 does not seem to form

phorate sulfone or phoratoxon that could be postulated as intermediate products on the route leading to phoratoxon sulfone (3) and phoratoxon sulfoxide (4), respectively as shown in Figure S1. For this reason, a reaction with only CYP3A4 using phorate as substrate was also carried out (Figure S1). In this case, phorate sulfoxide (2) and phoratoxon sulfone (3) were detected confirming that only the tandem reaction leads to the formation of phoratoxon sulfoxide (4) and that no observable intermediate product is formed in the CYP3A4 mediated transformation.

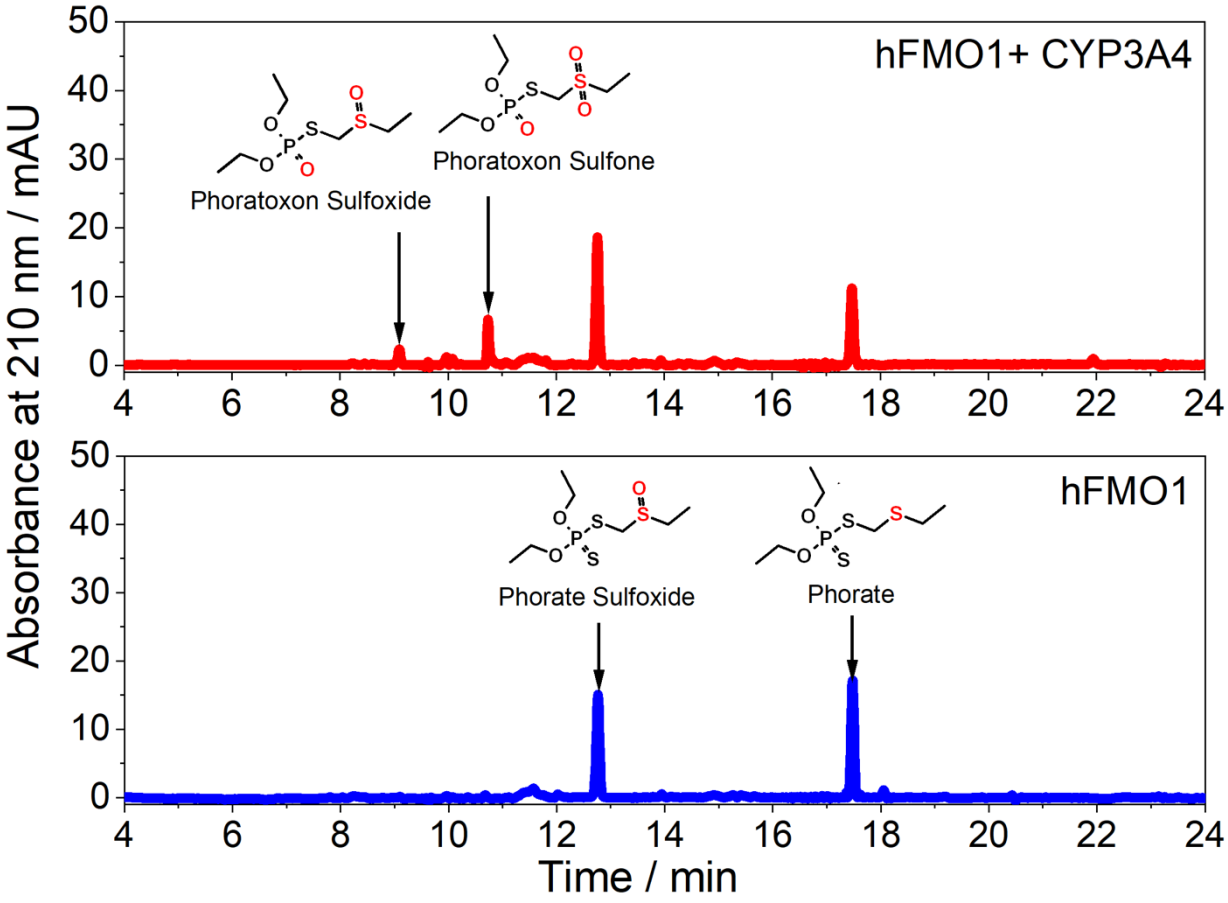

Figure 9. HPLC separations of the products of electrochemically driven reactions of hFMO1 (bottom, blue trace) and hFMO1 in tandem with CYP3A4 (top, red trace) with organophosphate pesticide phorate. Each sample contained 500 µM of phorate in 0.1 M phosphate buffer pH 7.4 with 0.1 M KCl as supporting electrolyte. The two enzymes were immobilized on glassy carbon electrodes as described within the text. Retention times are: phorate 17.2 min, phorate sulfoxide 12.7 min, phoratoxon sulfone 10.8 min and phoratoxon sulfoxide 9.0 min.

4. Conclusions

Xenobiotic metabolism is a complex process involving different enzymes often acting in sequence. It would be particularly interesting to have an in vitro platform able to mimic this complex process. As a step in this direction the data presented in this paper demonstrates the feasibility of using bioelectrodes with separately immobilised hFMO1 and CYP3A4, successfully carrying out their tandem reactions in the conversion of phorate, an organophosphate pesticide. These bioelectrochemical conversions not only lead to the single phorate sulfoxide product of hFMO1 but also the phoratoxon sulfoxide, the tandem enzymatic product of FMO1 followed by CYP3A4. These preliminary data are encouraging and lead the way to construct microfluidic systems which go beyond the single enzyme cell [50], by using several enzymes immobilised in a sequential format representing the detoxification pathways of xenobiotics within the human body.

Declaration of Competing Interest

The authors declare that they have no known competing financial interests or personal relationships that could have appeared to influence the work reported in this paper.

Acknowledgement

The authors wish to thank Claudia Grillo (University of Torino) for the expression and purification of the cytochrome P450 3A4. Hanna Cheropkina is the recipient of a three-year PhD scholarship from University of Torino awarded to international students.

Funding

This research did not receive any specific grant from funding agencies in the public, commercial, or not-for-profit sectors.

Author contributions

Conception and design of the study: SJS; Resources: GG, SJS; Acquisition of data: HC, GC, AM, FC; Analysis and interpretation of data: HC, GC, FC, SJS; Drafting the article: HC, GC, SJS; Review and editing: GG, SJS

References

[1] I. Mahmood, S.R. Imadi, K. Shazadi, A. Gul, K.R. Hakeem, Effects of Pesticides on Environment, in: K.R. Hakeem, M.S. Akhtar, S.N.A. Abdullah (Eds.), Plant, Soil and Microbes: Volume 1: Implications in Crop Science, Springer International Publishing, Cham, 2016: pp. 253–269. https://doi.org/10.1007/978-3-319-27455-3_13.

[2] A. Sabarwal, K. Kumar, R.P. Singh, Hazardous effects of chemical pesticides on human health–Cancer and other associated disorders, Environmental Toxicology and Pharmacology, 63 (2018) 103-114, https://doi.org/10.1016/j.etap.2018.08.018.

[3] R. Betarbet, T.B. Sherer, G. MacKenzie, M. Garcia-Osuna, A.V. Panov, J.T. Greenamyre, Chronic systemic pesticide exposure reproduces features of Parkinson's disease, Nature Neuroscience. 3 (2000) 1301–1306. https://doi.org/10.1038/81834.

[4] A. Ascherio, H. Chen, M.G. Weisskopf, E. O'Reilly, M.L. McCullough, E.E. Calle, M.A. Schwarzschild, M.J. Thun, Pesticide exposure and risk for Parkinson's disease, Annals of Neurology. 60 (2006) 197–203. https://doi.org/10.1002/ana.20904.

[5] K.M. Hayden, M.C. Norton, D. Darcey, T. Østbye, P.P. Zandi, J.C.S. Breitner, K.A. Welsh-Bohmer, Occupational exposure to pesticides increases the risk of incident AD: The Cache County Study, Neurology. 74 (2010) 1524–1530. https://doi.org/10.1212/WNL.0b013e3181dd4423.

[6] J.R. Richardson, A. Roy, S.L. Shalat, R.T. von Stein, M.M. Hossain, B. Buckley, M. Gearing, A.I. Levey, D.C. German, Elevated Serum Pesticide Levels and Risk for Alzheimer Disease, JAMA Neurology. 71 (2014) 284–290. https://doi.org/10.1001/jamaneurol.2013.6030.

[7] European Commission. Council Directive 98/83/EC of 3 November 1998 on the Quality of Water Intended for Human Consumption. 1998; p 18.

[8] M.C. Henderson, S.K. Krueger, L.K. Siddens, J.F. Stevens, D.E. Williams, S-oxygenation of the thioether organophosphate insecticides phorate and disulfoton by human lung flavin-containing monooxygenase 2. Biochem Pharmacol. 68(2004):959-67. https://doi.org/10.1016/j.bcp.2004.05.051.

[9] E. Hodgson, R.L. Rose, D.Y. Ryu, G. Falls, B.L. Blake, P.E. Levi. Pesticide-metabolizing enzymes. Toxicol Lett. 1995 Dec;82-83:73-81. https://doi.org/10.1016/0378-4274(95)03469-2.

[10] G. Denisov, T. M. Makris, S. G. Sligar, I. Schlichting, Structure and chemistry of cytochrome P450. Chem. Rev. 105 (2005) 2253–2278. https://doi.org/10.1021/cr0307143.

[11] J.R. Cashman, Structural and catalytic properties of the mammalian flavin-containing monooxygenase, Chem. Res. Toxicol. 8 (1995) 165–181. https://doi.org/10.1021/tx00044a001.

[12] D.M. Ziegler, An overview of the mechanism, substrate specificities and structure of FMOs, Drug Metab. Rev. 34 (2002) 503–511, https://doi.org/10.1081/DMR-120005650.

[13] W.C. Dauterman, Biological and nonbiological modifications of organophosphorus compounds, Bull World Health Organ 44 (1971) 133-150.

[14] N.P. Hajjar, E. Hodgson, Flavin adenine dinucleotide--dependent monooxygenase: its role in the sulfoxidation of pesticides in mammals, Science. 209 (1980) 1134–1136. https://doi.org/10.1126/science.7403873.

[15] B. Furnes, D. Schlenk, Extrahepatic metabolism of carbamate and organophosphate thioether compounds by the flavin-containing monooxygenase and cytochrome p450 systems, Drug Metab Dispos. 33 (2005) 214–218. https://doi.org/10.1124/dmd.104.000984.

[16] B. Furnes, D. Schlenk, Evaluation of xenobiotic n- and s-oxidation by variant flavin-containing monooxygenase 1 (FMO1) enzymes, Toxicological Sciences. 78 (2004) 196–203.

https://doi.org/10.1093/toxsci/kfh079.
[17] K.A. Usmani, E.D. Karoly, E. Hodgson, R.L. Rose, In Vitro Sulfoxidation of Thioether Compounds by Human Cytochrome P450 and Flavin-Containing Monooxygenase Isoforms with Particular Reference to the Cyp2c Subfamily, Drug Metab Dispos. 32 (2004) 333–339. https://doi.org/10.1124/dmd.32.3.333.
[18] S.J. Sadeghi, S. Ferrero, G. Di Nardo, G. Gilardi, Drug–drug interactions and cooperative effects detected in electrochemically driven human cytochrome P450 3A4,Bioelectrochemistry 86 (2012) 87–91. https://doi.org/10.1016/j.bioelechem.2012.02.010
[19] S.J. Sadeghi, A. Fantuzzi, G. Gilardi, Breakthrough in P450 bioelectrochemistry and future perspectives, Biochimica et Biophysica Acta 1814 (2011) 237–248. https://doi.org/10.1016/j.bbapap.2010.07.010
[20] P. Panicco, S. Castrignanò, S.J. Sadeghi, G. Di Nardo, G. Gilardi. Engineered human CYP2C9 and its main polymorphic variants for bioelectrochemical measurements of catalytic response. Bioelectrochemistry 38 (2021)107729. doi: 10.1016/j.bioelechem.2020.107729.
[21] R.C. Alkire, P.N. Bartlett, J. Lipkowski, Nanopatterned and Nanoparticle-Modified Electrodes; John Wiley & Sons, 2017; ISBN 978-3-527-34096-5.
[22] M. Pumera, Graphene in biosensing, Materials Today 14 (2011) 308–315. https://doi.org/10.1016/S1369-7021(11)70160-2.
[23] M. Pumera, Electrochemistry of graphene, graphene oxide and other graphenoids: Review, Electrochemistry Communications. 36 (2013) 14-18. https://doi.org/10.1016/j.elecom.2013.08.028.
[24] P.R. Aranda, G.A. Messina, F.A. Bertolino, S.V. Pereira, M.A. Fernández Baldo, J. Raba, Nanomaterials in fluorescent laser-based immunosensors: Review and applications, Microchemical Journal 141 (2018) 308-323. https://doi.org/10.1016/j.microc.2018.05.024
[25] S. Castrignanò, G. Gilardi, S.J. Sadeghi, Human flavin-containing monooxygenase 3 on graphene oxide for Drug Metabolism Screening, Anal. Chem. 87 (2015) 2974–2980. https://doi.org/10.1021/ac504535y.
[26] S. Castrignanò, S. Bortolussi, G. Catucci, O. Gholami, F. Valetti, G. Gilardi, S.J. Sadeghi, Bioelectrochemical profiling of two common polymorphic variants of human FMO3 in presence of graphene oxide, Electrochimica Acta. 228 (2017) 611–618. https://doi.org/10.1016/j.electacta.2017.01.131.
[27] C. Gao, G. Catucci, S. Castrignano, G. Gilardi, S.J. Sadeghi, Inactivation mechanism of N61S mutant of human FMO3 towards trimethylamine Sci. Rep. 7 (2017) 14668. https://doi.org/10.1038/s41598-017-15224-9
[28] H. Cheropkina, G. Catucci, A. Marucco, I. Fenoglio, G. Gilardi, S. J. Sadeghi, Human flavin-containing monooxygenase 1 and its long-sought hydroperoxyflavin intermediate, Biochemical Pharmacology 193 (2021) 114763. https://doi.org/10.1016/j.bcp.2021.114763
[29] G. Catucci, I. Polignano, D. Cusumano, C. Medana, G. Gilardi, S.J. Sadeghi, Identification of human flavin-containing monooxygenase 3 substrates by a colorimetric screening assay, Analytical Biochemistry. 522 (2017) 46–52. https://doi.org/10.1016/j.ab.2017.01.024.
[30] F. Zheng, X.-Y. Yang, P.-Q. Bi, M.-S. Niu, C.-K. Lv, L. Feng, X.-T. Hao, K. P. Ghiggino, Improved compatibility of DDAB-functionalized graphene oxide with a conjugated polymer by isocyanate treatment, RSC Advances. 7 (2017) 17633–17639. https://doi.org/10.1039/C6RA28652F.
[31] S.J. Sadeghi, R. Meirinhos, G. Catucci, V. R. Dodhia, G. Di Nardo, G. Gilardi, Direct Electrochemistry of Drug Metabolizing Human Flavin-Containing Monooxygenase: Electrochemical Turnover of Benzydamine and Tamoxifen. J. AM. CHEM. SOC. 132 (2010)

458–459. https://doi.org/10.1021/ja909261p
[32] D. Degregorio, S. D'Avino, S. Castrignanò, G. Di Nardo, S. J. Sadeghi, G. Catucci, G. Gilardi, Human Cytochrome P450 3A4 as a Biocatalyst: Effects of the Engineered Linker in Modulation of Coupling Efficiency in 3A4-BMR Chimeras, Front. Pharmacol. 8 (2017) 121. https://doi.org/10.3389/fphar.2017.00121
[33] V.R. Dodhia, C. Sassone, A. Fantuzzi, G. Di Nardo, S. J. Sadeghi, G. Gilardi, Modulating the coupling efficiency of human cytochrome P450 CYP3A4 at electrode surfaces through protein engineering, Electrochemistry Communications 10 (2008) 1744–1747. https://doi.org/10.1016/j.elecom.2008.09.007
[34] Fukuto TR. Mechanism of action of organophosphorus and carbamate insecticides, Environ Health Perspect 87 (1990) 245-254. https://doi.org/10.1289/ehp.9087245
[35] F. Arduini, A. Amine, D. Moscone, G. Palleschi. Biosensors based on cholinesterase inhibition for insecticides, nerve agents and aflatoxin B1 detection. Microchim Acta (2010) 170:193–214. https://doi.org/10.1007/s00604-010-0317-1.
[36] Commission Implementing Regulation (EU) 2019/1606 of 27 September 2019. EUR-Lex. 2019-09-30.
[37] P.E. Levi, E. Hodgson, Stereospecificity in the oxidation of phorate and phorate sulphoxide by purified FAD-containing mono-oxygenase and cytochrome P-450 isozymes, Xenobiotica. 18 (1988) 29–39. https://doi.org/10.3109/00498258809055134.
[38] C. Leoni, F.M. Buratti, E. Testai, The participation of human hepatic P450 isoforms, flavin-containing monooxygenases and aldehyde oxidase in the biotransformation of the insecticide fenthion, Toxicology and Applied Pharmacology. 233 (2008) 343–352. https://doi.org/10.1016/j.taap.2008.09.004.
[39] S. Castrignanò, S.J. Sadeghi, G. Gilardi, Electro-catalysis by immobilized human flavin-containing monooxygenase isoform 3 (hFMO3), Anal. Bioanal. Chem. 398 (2010) 1403–1409, http://dx.doi.org/10.1007/s00216-010-4014-z.
[40] S. Castrignanò, S.J. Sadeghi, G. Gilardi, Entrapment of human flavin-containing monooxygenase 3 in the presence of gold nanoparticles: TEM, FTIR and electrocatalysis, Biochim.Biophys. Acta 1820 (12) (2012) 2072–2078. http://dx.doi.org/10.1016/j.bbagen.2012.09.017.
[41] W.A. Khalil, H.H.A. Sherif, B. A. Hemdan, S. K.H. Khalil, W. El Hotaby. Biocompatibility enhancement of graphene oxide-silver nanocomposite by functionalisation with polyvinylpyrrolidone. IET nanobiotechnol. 2019. https://doi.org/10.1049/iet-nbt.2018.5321.
[42] G. Catucci, G. Gilardi, L. Jeuken, S.J. Sadeghi, In vitro drug metabolism by C-terminally truncated human flavin-containing monooxygenase 3, Biochemical Pharmacology. 83 (2012) 551–558. https://doi.org/10.1016/j.bcp.2011.11.029.
[43] D. Scarano, S. Bertarione, F. Cesano, G. Spoto, A. Zecchina, Imaging polycrystalline and smoke MgO surfaces with atomic force microscopy: a case study of high resolution image on a polycrystalline oxide, Surface Science 570,3 (2004) 155-166; https://doi.org/10.1016/j.susc.2004.07.024.
[44] F.M. Borodich, X. Jin, A. Pepelyshev. Probabilistic, Fractal, and Related Techniques for Analysis of Engineering Surfaces. Front. Mech. Eng. 6 (2020). https://doi.org/10.3389/fmech.2020.00064
[45] B. Han, Y. Zhao, C. Ma, C. Wang, X. Tian, Y. Wang, W. Hu, P. Samorì, Asymmetric chemical functionalization of top-contact electrodes: Tuning the charge injection for high-performance MoS2 field-effect transistors and Schottky Diodes, Advanced Materials 34 (2022) 12, 2109445. https://doi.org/10.1002/adma.202109445

[46] J. Kim, L.J. Cote, F. Kim, W. Yuan, K.R. Shull, J. Huang, Graphene Oxide Sheets at Interfaces Journal of the American Chemical Society, 132 (2010) 8180-8186, https://doi.org/10.1021/ja102777p
[47] H.-W. Tien , Y.-L. Huang , S.-Y. Yang , S.-T. Hsiao , W.-H. Liao , H.-M. Li , Y.-S. Wang , J.-Y. Wang. C.-C. M. Ma , Preparation of transparent, conductive films by graphene nanosheet deposition on hydrophilic or hydrophobic surfaces through control of the pH value J. Mater. Chem., 2012, 22 , 2545-2552. https://doi.org/10.1039/C1JM14564A
[48] S-T. Hsiao, C-C M. Ma, W-H. Liao, Y-S. Wang, S-M. Li, Y-C. Huang, R-B. Yang, W-F. Liang, Lightweight and Flexible Reduced Graphene Oxide/Water-Borne Polyurethane Composites with High Electrical Conductivity and Excellent Electromagnetic Interference Shielding Performance. ACS Applied Materials & Interfaces 6 (2014), 10667-10678. https://doi.org/10.1021/am502412q
[49] E. Laviron, L. Roullier, C. Degrand, A multilayer model for the study of space distributed redox modified electrodes: Part II. Theory and application of linear potential sweep voltammetry for a simple reaction, Journal of Electroanalytical Chemistry and Interfacial Electrochemistry. 112 (1980) 11–23. https://doi.org/10.1016/S0022-0728(80)80003-9.
[50] A. Fantuzzi, E. Capria, L. H. Mak, V. R. Dodhia, S. J. Sadeghi, S. Collins, G. Somers, E. Huq, G. Gilardi, An electrochemical microfluidic platform for human P450 drug metabolism profiling, Analytical Chemistry 82 (2010), 10222-10227. https://doi.org/10.1021/ac102480k.